

Research on Hydraulic Looper System Modeling and RBF Neural Network Decoupling Control

Dong Hui, Li Boqun, Zhang Shenglin, Yan Qinglun

School of Electronic and Information Engineering, University of Science and Technology Liaoning, China, Liaoning, Anshan, 114051
(Tel:+8618741270133; E-mail:1445725128@qq.com; lbqhylyxab@163.com; zsl171231@163.com; 939591018@qq.com)

Abstract: With the development of industry, in the production process, there are increasingly higher requirements for product accuracy and performance. However, there are serious coupling and strong uncertainty in complex engineering, especially in multivariable systems, the design is more complicated. Multivariable systems can choose a variety of algorithms to optimize parameters of complex models, including particle swarm optimization algorithm, genetic algorithm, and ant colony algorithm. This article introduces the RBF neural network based on the improved weed optimization algorithm into the coupled control system. It introduces the RBF neural network optimized by the improved weed algorithm into the coupled control system. On the basis of the state space dynamic model, using the two advantages of the weed algorithm's strong population competitiveness and wide spatial distribution range, the accuracy of the perceptron of the RBF neural network is accurately optimized, and finally the actual engineering is better controlled. It overcomes the problems of the basic weed algorithm (IWO) that are easy to fall into the local optimum, low convergence accuracy, and slow convergence speed. Finally, comparison are made with other optimization algorithms. The simulation results show the effectiveness of this method. The control scheme has high robustness to meet certain external disturbance coupling, and at the same time minimizes the relationship between the coupling variables, and the control effect has been significantly improved.

Keywords: Weed optimization algorithm; RBF neural network; complex system modeling; multivariable system decoupling

1. INTRODUCTION

In modern hot rolling mills, the control of the looper system is a very critical link, and its performance directly affects the width accuracy, thickness accuracy and shape accuracy of the finished strip. Looper can well guarantee the stability of rolling, so the establishment of looper model is very critical to its control effect. The purpose of looper system is to realize two adjacent rolling mills on the basis of low-tension rolling, and keep the metal seconds to flow rate of adjacent standers equal approximately.

When the strip enters the finishing rolling system, the forward slip generated is a function related to the incoming material inlet thickness, outlet thickness, and front and back tensile stress. When adjusting the roll gap, the loop height will be formed through the influence of forward and backward slipping. The control system detects the change of the swing angle of the looper. On the one hand, the roller speed is controlled to keep the loop height unchanged. On the other hand, the hydraulic looper is controlled to keep the rolling under small tension. During the swinging process of the hydraulic looper arm, there is an angular acceleration to form a dynamic moment. The dynamic torque is proportional to the moment of inertia of the looper system. It makes the tension torque change, and then affects the tension. The change of tension affects the loop height through the change of backward slip. Therefore, it is extremely important to realize the decoupling control of the looper system.

The response time and control accuracy of traditional looper control systems are characterized by nonlinearity and uncertainty. The accuracy can be further improved, but the coupling is strong, and it is difficult to obtain an accurate mathematical model. Due to the simplicity of PID control theory, the PID control scheme has been widely used in looper control systems. The traditional PID looper control system is a double closed loop control, using PID and PI to control the strip tension and looper angle respectively. However, the PID-based looper control system cannot solve the coupling problem between looper dynamics and tension dynamics. In the cases of interference and inaccurate modeling dynamic changes, it will lead to a long time to reach stability, and the tension and looper angle are both larger than expected. The traditional PID looper control system cannot effectively overcome model mismatch and unknown disturbances and parameter changes.

A robust controller is designed to improve the control accuracy (see Li and Wang J J et al., 2020). (Li and Zhang S L et al., 2020) using RBF-PID control strategy to improve thickness control accuracy. (Li et al., 2016) using two filters to smooth control signal and to suppress output noise. The identification accuracy and convergence speed of complex systems cannot be considered at the same time in the above three articles. Based on the establishment of the looper model. This paper uses the characteristics of the neural network that can approximate any nonlinear function, and

introduces the RBF neural network into the looper coupling control system. In order to give the weight of the better neural network, here we improve the basic weed optimization algorithm to improve its convergence, and by overcoming the shortcomings of easy falling into local optimum, to improve the control accuracy and speed. Finally, it is compared with ordinary differential evolution algorithm, particle swarm algorithm, genetic algorithm, and basic weed optimization algorithm. According to the simulation results, the improved weed optimization algorithm can increase the convergence speed and achieve better performance.

2. LOOPER SYSTEM MODELING

2.1 Production of strip tension

In the process of hot rolling strip, the reason why the tension of the rolled piece occurs is that the speed of the front and back standers are not equal, which lead to the imbalance of the metal flow mass. Resulting in the relative displacement of the metal in different parts of the rolled piece.

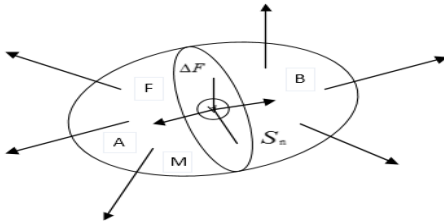


Fig. 1. Causes of stress.

As shown in Fig. 1, the object in equilibrium under the action of force F is divided into two parts. ΔF is a section on the F . The ratio of ΔF to the force ΔP acting on ΔF is:

$$\Delta S = \frac{\Delta F}{\Delta P} \quad (1)$$

According to Hooke's law, the relationship between stress and elastic strain is expressed as:

$$\sigma = E\varepsilon \quad (2)$$

In the formula, σ is the metal stress, E is the Young's modulus, and ε is the elastic deformation. Strip tension formula can be expressed as:

$$T = A\sigma_m \quad (3)$$

Where, σ_m is the tension of average unit. It can be seen from the above that the fundamental reason why the rolled piece produces tension is the elastic deformation of the rolled piece. As shown in Fig. 2, the elastic deformation formula can be expressed as:

$$\varepsilon = \frac{\Delta l}{l_0} \quad (4)$$

Where, Δl represents the relative displacement between points a and b due to the speed difference, and l_0 represents the distance between points a and b .

Substituting (2) and (4) into (3) to get the tension formula of rolled piece:

$$T_0 = A \cdot \sigma_{or} = \frac{AE}{l_0} \int (v_a - v_b) dt \quad (5)$$

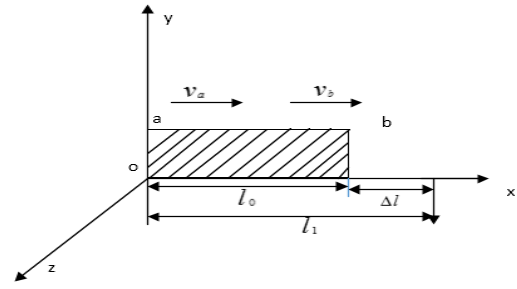


Fig. 2. Causes of tension in rolled piece.

In addition to the speed difference between point a and point b , point a and point b also have their own speed difference ,the tension T of rolled piece is:

$$T = T_0 + \Delta T = \frac{AE}{l_0} \int (v_a - v_b) dt + \frac{AE}{l_0} \int (\Delta v_a - \Delta v_b) dt \quad (6)$$

Where, Δv_a and Δv_b are the velocity changes of the two points themselves. It can be seen from the analysis of Eq. 6, either the average tension in the rolled piece or the tension in the rolled piece both are caused by the difference in velocity between points a and b , and the change in their own velocity. It has nothing to do with the velocity of points a and b . Therefore, it can be concluded that the influence factor of rolling tension is the sum of different speeds of different points in the rolled piece.

2.2 Looper Tension System Modeling

When the rolled piece enters the finishing mill and forms a stable hot continuous rolling, the tension of the rolled piece will have a relative change. There are two main factors, one is the change of the strip speed; the other is the change of the looper quantity. The variation of strip tension can be expressed as:

$$\Delta \sigma_i = \frac{E}{l_0} \left[\Delta L(\theta)_i + \int_0^l (\Delta v_{in,i+1} - \Delta v_{out,i}) dt \right] \quad (7)$$

Where, $\Delta L(\theta)_i$ is the variation of loop height. $\Delta v_{in,i+1}, \Delta v_{out,i}$ are the rolling speed at the entrance of $i+1$ th stander and the rolling speed at the exit of i th stand. The loop height between the i th and $i+1$ th stands can be expressed as:

$$L_i = \sqrt{(L_1 + R \cos \theta)^2 + (R \sin \theta - L_3 + r)^2} + \sqrt{(L - L_1 - R \cos \theta)^2 + (R \sin \theta - L_3 + r)^2} - L \quad (8)$$

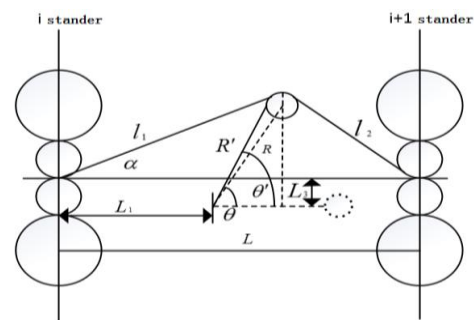


Fig. 3. Schematic diagram of looper between standers.

2.2.1 Tension changes caused by speed changes

The backward slip of $i+1$ th stander is:

$$b_{i+1} = \frac{v_{i+1} + v_{m,i+1}}{v_{i+1}} \quad (9)$$

Where, b_{i+1} is the height of backward slip; v_{i+1} is strip speed. According to (9), the speed variation of $i+1$ th stander can be expressed as:

$$\Delta v_{m,i+1} = (1 - b_{i+1})v_{i+1} - \Delta b_{i+1}v_{i+1} \quad (10)$$

In the same way, the change in forward slip speed can be expressed as:

$$\Delta v_{out,i} = (1 - f_i)v_i - \Delta f_i v_i \quad (11)$$

Incorporating (10) and (11) into (7) for differential arrangement, we can get:

$$\frac{d\Delta\sigma_i}{dt} = -\frac{E}{L}(1 + f_i)\Delta v_i - \frac{E}{L}\left(\frac{\partial b_{i+1}}{\partial\Delta\sigma_i}v_{i+1} + \frac{E}{L}\frac{\partial\Delta f_i}{\partial\Delta\sigma_i}v_i\right)\Delta\sigma_i \quad (12)$$

$$K_{v\sigma} = \frac{\partial b_{i+1}}{\partial\sigma_i}v_{i+1} + \frac{E}{L}\frac{\partial\Delta f_i}{\partial\sigma_i}v_i \quad (13)$$

Substituting (13) into (12) to get the change of tension as:

$$\Delta\sigma_i = -\frac{E}{sL}\left[(1 + f_i)\Delta v_i + K_{v\sigma}\Delta\sigma_i\right] \quad (14)$$

The variation of strip tension caused by the change of loop height can be expressed as:

$$\Delta\sigma_i(S) = \frac{E}{L}\Delta L_i(\theta)$$

$$\Delta L_i = \frac{d\Delta L_i}{d\theta}\Delta\theta(s)$$

$$\Delta\sigma_i(s) = \frac{E}{L}\frac{d\Delta L_i}{d\theta}\Delta\theta(s)$$

In summary:

$$\Delta\sigma_i = \frac{E}{sL}\frac{dL_i}{d\theta}\Delta\dot{\theta}(s) - \frac{E}{sL}\left[(1 + f_i)\Delta v_i + K_{v\sigma}\Delta\sigma_i\right]$$

2.2.2 Change of tension caused by change of loop height

The force load on the looper roller can be decomposed into the radial force FR and the tangential force FT . The radial force FR load on looper rotation has no effect on the loop angular velocity. The tangential force FT can be divided into the following parts: the interstand tension load on the looper roller F_{iT} , the strip bending force and strip gravity F_{bfgT} , the strip centrifugal force $F_{s,cfT}$, the strip inertia force $F_{s,ifT}$ and the looper roll inertia force $F_{l,ifT}$, and the tangential force FT can be expressed as:

$$F_T = F_{iT} + F_{bfgT} + F_{s,cfT} + F_{s,ifT} + F_{l,ifT} \quad (15)$$

1) With rigid intermediate tension

According to the geometrical relationship shown in Fig. 3, the interstand tension in the tangential direction F_{iT} can be expressed as:

$$F_{iT} = \sigma wh \left[\sin(\theta + \theta_2) - \sin(\theta + \theta_1) \right] \quad (16)$$

Where, H is the gauge of strip steel, W is the width of strip.

2) Strip bending force and strip gravity

The bending force and gravity in the tangential direction can be calculated as:

$$F_{bfgT} = \left[16E \cdot w(L_3 \sin\theta - L_1 + r) \cdot \left(\frac{h}{l}\right)^3 + \frac{1}{2}W_s \cdot g + W_R \cdot g \right] \cos\theta \quad (17)$$

Where g is the acceleration due to gravity, W_s is the mass of the strip, and W_R is the mass of the looper roll.

3) Strip centrifugal force

As shown in Fig. 3, there is a partial contact area between the strip and the looper roll, and the tangential centrifugal force in the contact area can be calculated as

$$F_{s,cfT} = -(\theta_1 + \theta_2) \cdot w \cdot h \cdot \rho \cdot \omega_L^2 \cdot \cos\theta \quad (18)$$

4) Strip inertia force

The contact area between the strip steel and the looper rolls are divided into two parts, and the strip tangential inertia force of strip can be expressed as:

$$F_{s,ifT} = 0.25\omega_s L_3 \ddot{\theta} [\cos(\theta - \theta_1)]^2 + 0.25\omega_s L_3 \ddot{\theta} [\cos(\theta + \theta_2)]^2 \quad (19)$$

5) Looper roller inertia force

The direction of the inertial force of the looper roller is perpendicular to the direction of the looper swing arm, the inertial force of the looper roller does not exist in the radial direction, and the function of the inertial force is that the tangential force of the looper roller can be calculated as

$$F_{l,ifT} = W_R \cdot L_3 \cdot \ddot{\theta} \quad (20)$$

The looper angle dynamics behavior can be described by Newton law of motion, and the following equation can be expressed as:

$$J \ddot{\theta}(t) = M(t) - M_L(\theta) - c_f \dot{\theta}(t) \quad (21)$$

Where, J is the total inertia of the looper, $M(t)$ is the actuator torques on the looper, c_f is the friction, and $M_L(\theta)$ is the load torque on the looper:

$$M_L(\theta) = F_T(\theta) \cdot L_3 \quad (22)$$

Above all, substituting (16) - (20) into (21), dynamic model of the looper angle can be expressed as:

$$\ddot{\theta} = \frac{M - L_3 wh \sigma [\sin(\theta + \theta_2) - \sin(\theta - \theta_1)]}{0.25L_3^2 W_s \{ \cos(\theta - \theta_1)^2 + \cos(\theta + \theta_2)^2 \} + J + W_R (L_3)^2} - \frac{L_3 \cos\theta \left[16E \cdot w(L_3 \sin\theta - L_1 + r) \cdot \left(\frac{h}{l}\right)^3 + \frac{1}{2}W_s \cdot g + W_R \cdot g \right]}{0.25L_3^2 W_s \{ \cos(\theta - \theta_1)^2 + \cos(\theta + \theta_2)^2 \} + J + W_R (L_3)^2} - \frac{(\theta_1 + \theta_2) \cdot w \cdot h \cdot \rho \cdot \omega^2 \cdot L_3 \cdot \cos\theta + c_f \omega_L}{0.25L_3^2 W_s \{ \cos(\theta - \theta_1)^2 + \cos(\theta + \theta_2)^2 \} + J + W_R (L_3)^2} \quad (23)$$

2.3 Dynamic model of actuator

Always choose hydraulic pressure to adjust the looper, hydraulic system automatic torque regulator. Due to the fast speed of the auto-regulator, it can be modeled as a first-order system

$$\dot{M}(t) = -\frac{M(t)}{T_{cr}} + \frac{1}{T_{cr}} M_r(t) \quad (24)$$

Where, T_{cr} is the time constant of the first-order automatic torque regulator, and $M_r(t)$ is the reference value of the looper actuator torque. The work roll is directly driven by a high-speed motor and is equipped with an automatic speed regulator. It is also regarded as a first-order lag signal as:

$$\dot{\omega}(t) = -\frac{\omega(t)}{T_{md}} + \frac{1}{T_{md}} M(t) \quad (25)$$

Where, T_{md} is the time constant of the first-order automatic speed governor and $\omega_r(t)$ is the roll angular velocity reference.

2.4 State space model

Looper system has five state variables: looper angle θ , inter-belt tension σ , looper roll angular speed ω_L , work roll angular speed ω , and execute looper M . the equation of multivariable looper system can be expressed as:

$$\begin{aligned} \dot{\Delta\theta} &= \omega_L \\ \dot{\Delta\sigma} &= G_\sigma \cdot \Delta\sigma + G_{\omega_L} \cdot \Delta\omega_L + G_{\omega_i} \cdot \Delta\omega_i + G_{\omega_{i+1}} \cdot \Delta\omega_{i+1} \\ \dot{\Delta\omega_L} &= \frac{1}{J} (\Delta M + K_\sigma \cdot \Delta\sigma + K_\theta \cdot \Delta\theta) \\ \dot{\Delta\omega_i} &= -\frac{1}{T_{md,i}} \Delta\omega_i + \frac{1}{T_{md,i}} \Delta\omega_{r,i+1} \\ \dot{\Delta M} &= -\frac{\Delta M}{T_{cr}} + T_{cr} \Delta M_r \end{aligned} \quad (26)$$

$G_\sigma = -\frac{E v_i}{L} \frac{\partial f_i}{\partial \sigma} - \frac{E v_{i+1}}{L} \frac{\partial f_{i+1}}{\partial \sigma}$ is the influence coefficient of the strip tension on the strip speed;

$G_{\omega_L} = \frac{E dL_i}{L d\theta}$ is the influence coefficient of the looper angle on the looper speed

$G_{\omega_i} = -\frac{ER_i(1+f_i)}{L}$; $K_M = \frac{1}{J}$; $K_\theta = -\frac{\partial M}{\partial \theta}$ is the influence coefficient of the looper angle on looper torque.

$K_\sigma = -\frac{\partial M}{\partial \sigma}$ is the influence coefficient of the strip tension in the looper's torque.

Convert the above state space Eq. to matrix form as follows:

$$\begin{bmatrix} \dot{\Delta\theta} \\ \dot{\Delta\sigma} \\ \dot{\Delta\omega_L} \\ \dot{\Delta\omega_i} \\ \dot{\Delta M} \end{bmatrix} = \begin{bmatrix} 0 & 0 & 1 & 0 & 0 \\ 0 & G_\sigma & G_{\omega_L} & G_{\omega_i} & 0 \\ k_\theta & k_\sigma & 0 & 0 & k_M \\ 0 & 0 & 0 & -\frac{1}{T_{md,i}} & 0 \\ 0 & 0 & 0 & 0 & -\frac{1}{T_{cr}} \end{bmatrix} \begin{bmatrix} \Delta\theta \\ \Delta\sigma \\ \Delta\omega_L \\ \Delta\omega_i \\ \Delta M \end{bmatrix} + \begin{bmatrix} 0 & 0 \\ 0 & 0 \\ 0 & 0 \\ \frac{1}{T_{md,i}} & 0 \\ 0 & \frac{1}{T_{cr}} \end{bmatrix} \begin{bmatrix} \Delta\omega_{r,i} \\ \Delta M_r \end{bmatrix} \quad (27)$$

The output matrix of the multivariable looper system can be expressed as:

$$\begin{bmatrix} \Delta\theta \\ \Delta\sigma \\ \Delta\omega_L \\ \Delta\omega_i \\ \Delta M \end{bmatrix} = \begin{bmatrix} 1 & 0 & 0 & 0 & 0 \\ 0 & 1 & 0 & 0 & 0 \end{bmatrix} \begin{bmatrix} \Delta\theta \\ \Delta\sigma \\ \Delta\omega_L \\ \Delta\omega_i \\ \Delta M \end{bmatrix} \quad (28)$$

For the convenience of notation, the above matrix is rewritten as:

$$\begin{aligned} \dot{x}(t) &= Ax(t) + Bu(t) \\ y(t) &= Cx(t) \end{aligned} \quad (29)$$

$$\begin{aligned} x(t) &= [\Delta\theta \quad \Delta\sigma \quad \Delta\omega_L \quad \Delta\omega_i \quad \Delta M]^T, u(t) = [\Delta\omega_{r,i} \quad \Delta\omega_{r,i+1}]^T \\ y(t) &= [\Delta\theta \quad \Delta\sigma]^T \end{aligned} \quad (30)$$

The matrix satisfies the following formula that can be expressed as:

$$A = \begin{bmatrix} 0 & 0 & 1 & 0 & 0 \\ 0 & G_\sigma & G_{\omega_L} & G_{\omega_i} & 0 \\ k_\theta & k_\sigma & 0 & 0 & k_M \\ 0 & 0 & 0 & -\frac{1}{T_{md,i}} & 0 \\ 0 & 0 & 0 & 0 & -\frac{1}{T_{cr}} \end{bmatrix}, B = \begin{bmatrix} 0 & 0 \\ 0 & 0 \\ \frac{1}{T_{md,i}} & 0 \\ 0 & \frac{1}{T_{cr}} \end{bmatrix}, C = \begin{bmatrix} 0 & 1 \\ 1 & 0 \\ 0 & 0 \\ 0 & 0 \\ 0 & 0 \end{bmatrix} \quad (31)$$

Based on the linear looper model, the block diagram of multivariable looper system is given, as shown in Fig.4. The purpose of looper control system is to allow the system to track the output accurately and quickly by adjusting the input increment, and the output increment can be controlled near zero even in the case of large interference.

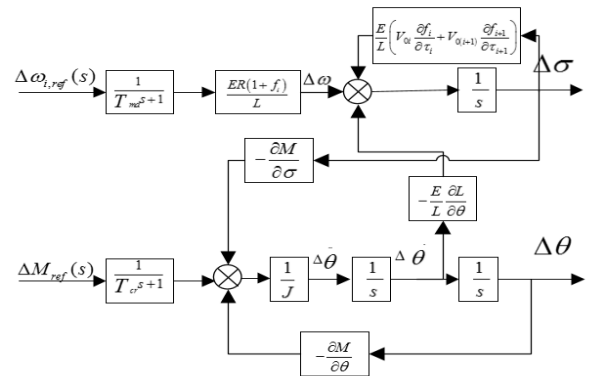


Fig. 4. Multivariable Looper System.

Table 1. Parameters of looper system of 1700mm hot rolling mill.

| Variable | Value | Unit | Variable | Value | Unit |
|----------|-------|-------|--------------------|--------|---------------------|
| E | 150 | Gpa | W_1 | 260 | kg |
| L | 5.5 | m | W_R | 370 | |
| f_i | 1.03 | % | W_S | 189.94 | |
| T_{md} | 0.2 | S | ω_r | 21.14 | Rad / s |
| T_{cr} | 0.03 | S | ∂f_i | 4.8 | N / mm ² |
| l | 6000 | mm | τb_i | 3.0 | |
| l_a | 2200 | mm | ∂f_{i+1} | 5.5 | N / mm ² |
| v_i | 3.246 | m / s | v_{i+1} | 4.786 | m / s |

$$V_{0i} \frac{\partial f_i}{\partial \tau_i} + V_{0(i+1)} \frac{\partial f_{i+1}}{\partial \tau_{i+1}} = 0.012$$

$$-\frac{\partial M}{\partial \theta} = -170.8; -\frac{\partial L}{\partial \theta} = -0.1066; -\frac{\partial M}{\partial \sigma} = -642$$

3. RBF NEURAL NETWORK

The RBF-Radial Basis Function (RBF) neural network is a neural network proposed by J. Moody and C. Darken in the late 1980s. It is a three-layer feed forward network with a single hidden layer. Since it simulates a neural network that is locally adjusted in the human brain and covers the receiving field (or receptive field), the graph of the radial basis function is shown in Fig. 5. It can be seen that the input signal n of the function is close to the function in the central range, hidden layer nodes produce larger output, so RBF network has local approximation ability (see Chen M X et al., 2021).

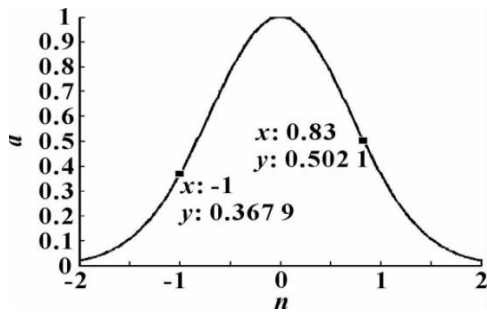


Fig. 5. Graph of radial basis function.

3.1 Network structure

The RBF network is a three-layer forward network. The mapping from input to output is nonlinear, while the mapping from hidden layer space to output space is linear. The output of the network is the linear weighted sum of the hidden layer node outputs, so the weight of the network can be solved by various linear optimization algorithms, which greatly accelerates the learning speed and avoids local minima problems.

The RBF network structure is shown in Fig. 6.

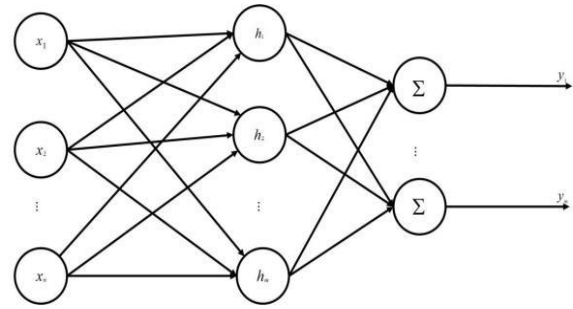


Fig. 6. RBF neural network structure.

3.2 RBF network PID tuning principle

RBF neural network has the ability of representing arbitrary non-linear and can realize PID control with the best combination by learning the system performance. Using PID control based on RBF neural network identification can realize decoupling control of multivariable systems. The controller consists of two parts: the classic PID controller and the RBF neural network identifier. The structure of the control system is shown in Fig. 7.

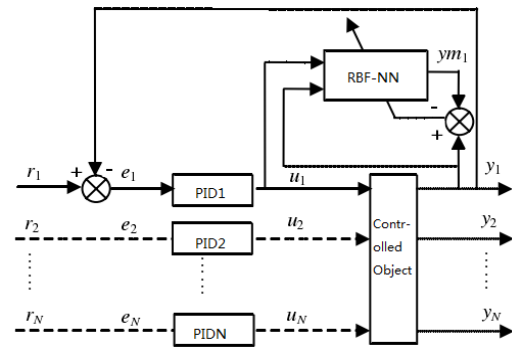


Fig. 7. Block diagram of the multi-variable PID decoupling control system.

1)Classic PID controller (see Long Z Q et al., 2004): Direct closed-loop control of the controlled object process, and the three parameters of K_p, K_i, K_d are set online. In order to achieve good control results for PID control, it is necessary to adjust the proportional, integral, and derivative controls to form a relationship that cooperates with each other and restricts each other in the control quantity. This relationship is not a necessarily simple linear combination, and the best relationship can be found from the infinitely variable nonlinear combination.

2)BRF Neural Network Identifier (see Dong W H et al., 2007): according to the operating state of the system, the nonlinear time-varying model of the system is identified online, and the PID controller parameters of each subsystem are automatically adjusted to achieve the optimization of a certain performance index. Finally, the intelligent decoupling control of the system is realized. Even if the output state of the output layer neuron corresponds to the three adjustable parameters of the PID controller, its stable state corresponds to the PID controller parameters under an optimal control law through the learning and weighting system adjustment of the neural network itself.

The dual-input, dual-output multi-variable self-tuning PID controller is shown in Fig. 8, where NN1 and NN2 are neural networks, because the PID parameters of controllers U_1 and U_2 are K_p, K_i, K_d . rin_1 and rin_2 are the designated inputs of the system, and $yout_1$ and $yout_2$ are the output values of the system.

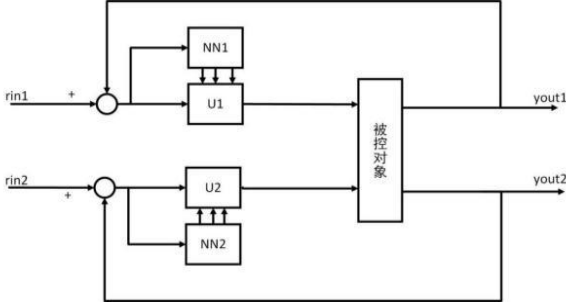


Fig. 8. PID controller with dual input and dual output tuning.

Using incremental PID controller, the control error is

$$error_1(k) = rin_1(k) - yout_1(k)$$

The three PID inputs are

$$\begin{aligned} xc_1(1) &= error_1(k) - error_1(k-1) \\ xc_1(2) &= error_1(k) \\ xc_1(3) &= error_1(k) - 2error_1(k-1) + error_1(k-2) \end{aligned} \quad (32)$$

The control algorithm is

$$\begin{aligned} u_1(k) &= u_1(k-1) + k_{p1}(error_1(k) - error_1(k-1)) + k_{i1}error_1(k) \\ &+ k_{d1}(error_1(k) - 2error_1(k-1) + error_1(k-2)) \end{aligned} \quad (33)$$

The neural network tuning index is

$$E_1(k) = \frac{1}{2} error_1(k)^2 \quad (34)$$

The adjustment of K_p, K_i, K_d adopts the gradient descent method

$$\Delta k_{p1} = -\eta_p \frac{\partial E_1}{\partial k_{p1}} = -\eta_p \frac{\partial E_1}{\partial y_1} \frac{\partial y_1}{\partial u_1} \frac{\partial u_1}{\partial k_{p1}} = \eta_p error_1(k) \frac{\partial y_1}{\partial u_1} xc_1(1) \quad (35)$$

$$\Delta k_{i1} = -\eta_i \frac{\partial E_1}{\partial k_{i1}} = -\eta_i \frac{\partial E_1}{\partial y_1} \frac{\partial y_1}{\partial u_1} \frac{\partial u_1}{\partial k_{i1}} = \eta_i error_1(k) \frac{\partial y_1}{\partial u_1} xc_1(2) \quad (36)$$

$$\Delta k_{d1} = -\eta_d \frac{\partial E_1}{\partial k_{d1}} = -\eta_d \frac{\partial E_1}{\partial y_1} \frac{\partial y_1}{\partial u_1} \frac{\partial u_1}{\partial k_{d1}} = \eta_d error_1(k) \frac{\partial y_1}{\partial u_1} xc_1(3) \quad (37)$$

In the formula, η_p, η_i, η_d are the PID parameter learning rate, and $\partial y / \partial u$ is the Jacobian information of the controlled object, which can be obtained through the identification of the neural network.

3.3 Identification algorithm of accused object Jacobian information

In the RBF network structure, $X = [x_1, x_2, \dots, x_n]^T$ is the input variable of the network. Suppose that the radial basis vector

of RBF network is $H = [h_1, h_2, \dots, h_j, \dots, h_m]^T$, where h_j is the Gaussian function

$$h_j = \exp\left(-\frac{\|X - C_j\|^2}{2b_j^2}\right) \quad j = 1, 2, \dots, m \quad (38)$$

The center vector of the j-th node of the network is

$$C_j = [c_{j1}, c_{j2}, \dots, c_{jn}, \dots, c_{jm}]^T$$

Suppose the basis width vector of the network is

$$B = [b_1, b_2, \dots, b_m]^T$$

b_j is the base width parameter of node j, and is a number greater than zero. The weight vector of the network is

$$W = [w_1, w_2, \dots, w_j, \dots, w_m]^T \quad (39)$$

The output of the identification network is

$$y_m(k) = w_1 h_1 + w_2 h_2 + \dots + w_m h_m \quad (40)$$

The performance index function of the identifier is

$$J_m = \frac{1}{2} (yout_1(k) - y_{m1}(k))^2$$

In the formula, y_{m1} is the output of the identifier.

According to the gradient descent method, an iterative algorithm for the parameters of output weight, node center and node base width is proposed

$$\begin{aligned} w_j(k) &= w_j(k-1) + \eta (yout_1(k) - y_{m1}(k)) h_j \\ &+ \alpha (w_j(k-1) - w_j(k-2)) \end{aligned} \quad (41)$$

$$\Delta b_j = (yout_1(k) - y_{m1}(k)) w_j h_j \frac{\|x - c_j\|^2}{b_j^3} \quad (42)$$

$$b_j(k) = b_j(k-1) + \eta \Delta b_j + \alpha (b_j(k-1) - b_j(k-2)) \quad (43)$$

$$\Delta C_{ji} = (yout_1(k) - y_{m1}(k)) w_j \frac{x_j - c_{ji}}{b_j^2} \quad (44)$$

$$C_{ji}(k) = C_{ji}(k-1) + \eta \Delta C_{ji} + \alpha (C_{ji}(k-1) - C_{ji}(k-2)) \quad (45)$$

In the formula, η is the learning rate and α is the momentum factor.

Jacobian matrix (that is, the sensitivity information of the output of the object to the control input) algorithm is

$$\frac{\partial y(k)}{\partial u_1(k)} = \frac{\partial y_{m1}(k)}{\partial u_1(k)} = \sum_{j=1}^m w_j h_j \frac{c_{ji} - x_j}{b_j^2} \quad (46)$$

Where, $x_1 = u_1(k)$

4. WEED OPTIMIZATION ALGORITHM

4.1 Basic weed optimization algorithm

Invasive Weed Optimization (see Mehrabian A R et al., 2006) (IWO) is proposed by A R Mehrabian et al. in 2006 to simulate the basic process of spatial diffusion, growth,

reproduction and competitive extinction of weed seeds with tenacious vitality in nature. This kind of bionic swarm intelligence algorithm is a meta-heuristic algorithm inspired by ecology. The algorithm has the characteristics of simple structure, fast convergence speed, parallel operation robustness and strong adaptability. Since it was put forward, it has attracted the attention of many scholars. At present, it has been applied in many aspects such as artificial neural network model optimization (see Giri R et al., 2010; Peng B et al., 2013; Dun X H et al., 2018). The IWO algorithm is an efficient random intelligent optimization algorithm. It uses excellent individuals in the group to guide the evolution of the population. And uses normal distribution to dynamically change the standard deviation to superimpose the offspring individuals produced by the excellent individuals around the parent individuals. The offspring individuals are produced and superimposed by the excellent individuals around the parent individuals by using normal distribution to dynamically change the standard deviation. The algorithm takes into account the diversity of the group and the strength of selection.

The main steps of the weed optimization algorithm are as follows:

Step 1 Initialize the population. The upper and lower limits of the variables are given, the D-dimensional initial solution is randomly generated in a uniformly distributed manner, and the basic parameters of the algorithm are initialized.

Step 2 Individual reproduction of offspring. Parents distributed in the entire search space produce next-generation seeds based on the fitness value of the parent. The number of offspring seeds is determined by the fitness value and has a linear relationship with the fitness value. Individuals with high fitness value produce more seeds. Individuals with low fitness values produce fewer seeds, as shown in Fig. 9.

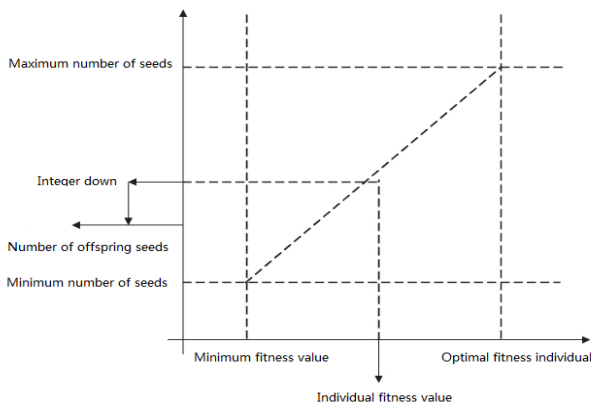


Fig. 9. Curve for determining the number of population seeds.

The number of offspring individuals is:

$$N = S_{\min} + \text{ceil}[(S_{\max} - S_{\min}) \frac{f_k - f_{\min}}{f_{\max} - f_{\min}}] \quad (47)$$

Where, S_{\min}, S_{\max} are the minimum and maximum numbers of offspring that the parent can produce; f_k is the individual fitness of the parent; f_{\min}, f_{\max} are the minimum and maximum fitness of the parent individual respectively.

Step 3 Space diffusion. The offspring individuals are distributed around the parent individuals according to a certain law, and the distribution position law satisfies the normal distribution.

The standard deviation change formula is:

$$\delta_k = [(M - t) / M]^n (\delta_{\text{initial}} - \delta_{\text{final}}) + \delta_{\text{final}} \quad (48)$$

Where, $iter_{\max}$ is the maximum evolutionary algebra; $iter$ is the current evolutionary algebra; n is the nonlinear harmonic factor, usually $n=3$.

Step 4 Competitive exclusion. After several generations of breeding operations, when the population size reaches the preset P_{\max} , the parents and offspring in the population are sorted, Selecting the better first P_{\max} according to the fitness value.

Repeat the above process until the optimal solution condition is satisfied or the maximum number of iterations is reached.

The flow chart of the basic weed optimization algorithm is shown in Fig. 10:

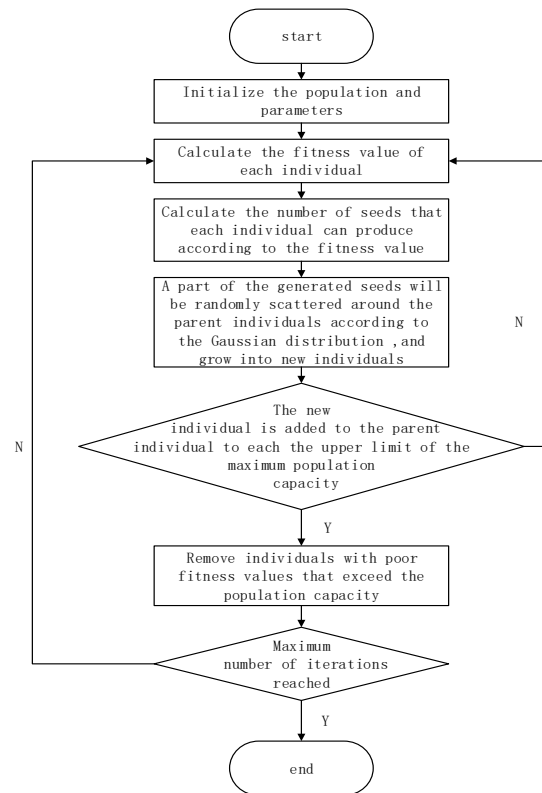


Fig. 10 Basic weed optimization algorithm steps

4.2 Improved weed optimization algorithm

The basic weed algorithm converges slowly in the later stages of evolution, and generates offspring around the parent in a Gaussian distribution. This search method has both depth and breadth, but most offspring produced by the Gaussian distribution are closer to the parent. May leads to a local optimum. Therefore, in each iteration, the population is equally divided into two parts. The first part produces offspring according to the Gaussian distribution, and the

second part produces offspring according to the Cauchy distribution. This spreads the space of the algorithm. Through this method, the space of the algorithm is diffused. Due to the strong local optimization ability of the weed algorithm, that is the weeds have the trend of tend to the local optimal weeds in the population. In order to slow down the simplification of the later weed population caused by this phenomenon and the algorithm searches speed decreases. This paper introduces a differential evolution strategy after the generation of new individuals, and performs mutation, crossover and selection operations on individuals to make them jump out of the local optimal situation and increase the diversity of the population. As shown in Fig. 11, individuals tend to fall into a search deadlock in a better position, but the differential evolution strategy can jump out of the local optimal situation, and then search for the global to obtain the global optimal.

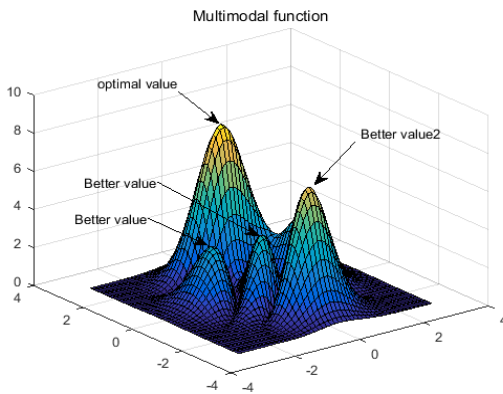


Fig. 11. Multimodal function.

4.2.1 Search space diffusion

The Gaussian density function of $f(x)$ obeys the distribution of

$$N(0,1) \text{ as: } f(x) = \frac{1}{\sqrt{2\pi}} e^{-\frac{x^2}{2}}$$

The Cauchy density function of $f(x)$ obeys the distribution of

$$C(0,1) \text{ as: } f(x) = \frac{1}{\pi(1+x^2)}$$

The two formulas of generating offspring can be described as:

$$P_{popk+1} = P_{popk} + \delta_k N(0,1) \quad (49)$$

$$P_{popk+1} = P_{popk} + \delta_k C(0,1) \quad (50)$$

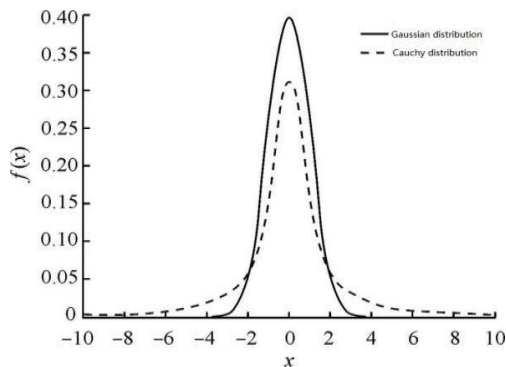


Fig. 12. Distribution curve of Gaussian and Cauchy distribution.

It can be seen from Fig. 12 that the Cauchy distribution has a relatively small peak in the vertical direction. In the horizontal direction, it changes more slowly when it is close to the horizontal axis. Compared with the Gaussian distribution, the Cauchy distribution is more likely to generate random numbers far away from the origin and has a wide range of random numbers. This allows the IWO algorithm to generate more diverse individuals at the initial stage, and it is easy to jump out of the local optimal or flat area. Both have their own advantages and disadvantages. For this reason, this article adopts a combination of the them.

The main steps of the improved weed optimization algorithm:

Step 1 Initialize the population and parameters, including the number of iterations, population number, maximum population number, number of offspring, nonlinear modulation index, standard deviation range, etc.

Step 2 Determine the standard deviation of offspring by (48), determine the number of offspring by (47), and generate offspring individuals according to (49) and (50).

Step 3 Calculate whether the total number of offspring individuals and parent individuals generated by the two distributions exceeds the maximum population size. If it exceeds, some individuals will be eliminated. Otherwise, the next generation of individuals will continue to be produced.

Step 4 Substitute the various groups into the neural network training model to calculate the fitness, and the parents and offspring compete for elimination.

Step 5 Judge whether the current iteration number has reached the maximum iteration number. If it reaches the maximum number of iterations, output the optimal individual as the neural network weight and threshold; otherwise, return to step 2.

4.2.2 Differential evolution strategy

Differential evolution algorithm (see Price K et al., 2006) mainly includes three typical evolutionary calculations: mutation, crossover, and selection. It has the advantages of memorizing individual optimal solutions, fewer controlled numbers, and strong global convergence in order to solve the shortcomings of IWO. The mutation, crossover, and selection operations of DE are introduced into IWO, and the specific operations are as follows:

Step 1 Seed mutation. The seed of the mutation operation after the spatial diffusion process is

$$U_i = X_{z1} + F(X_{z2} - X_{z3}) \quad (51)$$

Where, F is the scaling factor, $F \in [0,2]$; X_{z1}, X_{z2}, X_{z3} are the 3 seeds produced by weed X_i .

Step 2 Seed crossover. The crossover operation of the following formula is performed on $X_i(t)$ and $Y_i(t)$ of the t -th generation, which can further improve the diversity of the algorithm population.

$$U_{ij} = \begin{cases} Y_{i,j}(t) & \text{rand}(0,1) \leq CR \\ X_{i,j}(t) & \text{rand}(0,1) > CR \end{cases} \quad (52)$$

Where: CR is the crossover probability.

Step 3 Seed selection

$$X_i = \begin{cases} U_{i,j} & f(U_{i,j}) \leq f(X_i) \\ X_i & f(U_{i,j}) > f(X_i) \end{cases} \quad (53)$$

The algorithm flow chart is shown in Fig. 13:

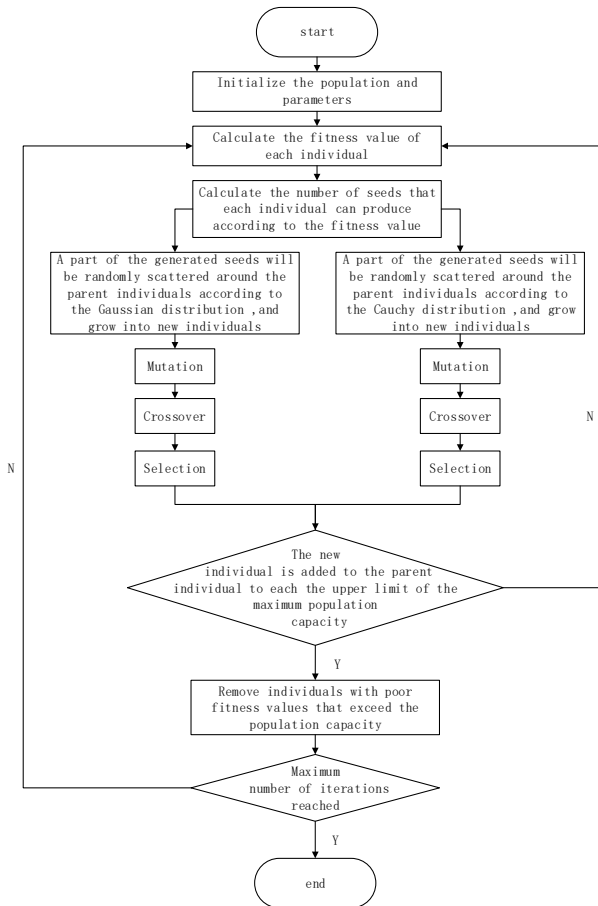


Fig. 13. Improved weed optimization algorithm steps.

5. SIMULATION AND ANALYSIS

5.1 Comparison of improved algorithms

Differential algorithm, particle swarms algorithm, genetic algorithm, basic weed algorithm and improved weed algorithm are applied to the optimization of RBF neural network. The sampling time of this system is set to the nearest 0.01s to the actual project. The sampling time is set as 0.01s which is closest to the actual project. The population size is 30 and the number of iterations is 50. The fitness curve of each optimization algorithm is as follows. (Fig. 14)

As shown in the above simulation diagram, comparing the convergence process of ordinary differential evolution algorithm, particle swarm algorithm, genetic algorithm, basic weed optimization algorithm and improved weed optimization algorithm, from the convergence trend analysis of its optimization performance, it can be seen that: ordinary differential evolution Algorithms, particle swarm optimization and genetic algorithms have the disadvantages

of premature and easy to fall into local optimization, and cannot increase the diversity of required weights.

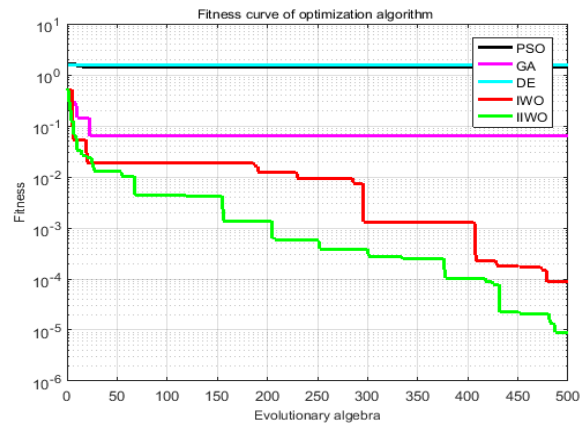


Fig. 14. Comprehensive simulation diagram.

There are contradictions in global optimization and local optimization, which cannot be considered at the same time. Although the basic weed optimization algorithm converged quickly in the early stage, it remained flat after converging to 260 generations. The improved weed optimization algorithm not only maintains the rapid convergence in the early stage, but also the model is still being optimized at the later stage. Comparing several optimization algorithms, the improved weed optimization algorithm has higher neural network accuracy and better optimization effect.

5.2 Traditional conventional PID decoupling

In order to verify the performance of the improved decoupling algorithm, the looper tension system is modeled and simulated. The conventional PID looper tension decoupling control is shown in Fig. 15. The decoupling control is realized in about 0.6 seconds, and the system is stable.

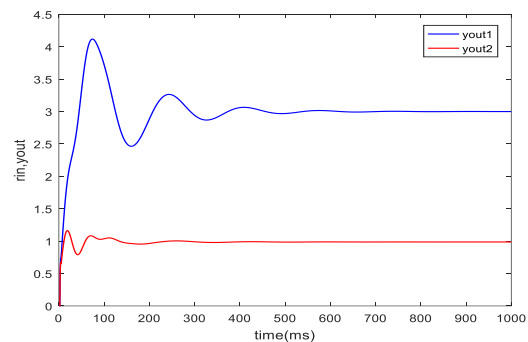


Fig. 15. Traditional PID looper tension decoupling control.

5.3 RBF neural network decoupling

From the simulation Fig. 16, it is known that the decoupling control is realized in about 0.2 seconds, and the system is stable.

It can be seen from the above simulation diagram that the rise time of the traditional PID decoupling control system is 74ms, the peak value is 4.117, the overshoot is 37.2%, and the system tends to be stable at 552ms. The RBF neural network

shows that there is no overshoot in the system from the simulation results.

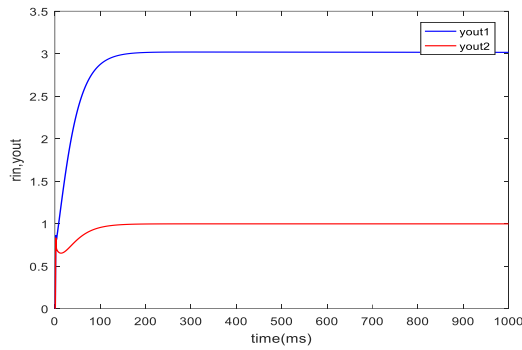


Fig. 16. Improved weed optimization algorithm decoupling control.

The system is completely decoupled at 186ms, and the system tends to be stable. Compared with PID adjustment, the time is shortened and the adjustment process is smoother. The oscillation amplitude is Obvious improvement has been made, which reduces the wear of the actuator and high-frequency execution in the actual field, and ensures that the rolling quickly enters the steady state. The fluctuation of the system and the time to reach the steady state is all due to the traditional PID control system.

5.4 System performance comparison

In the actual production process, there are often phenomena such as uncertainty and disturbance in the system. For example, temperature fluctuations will affect the change of the forward and backward slip coefficients, and then change the change of the looper and tension. A test sine function is selected here, and the performance is shown in Fig.17、 18.

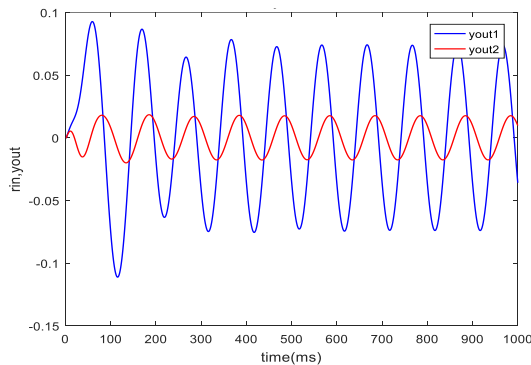


Fig. 17. Track sin sine signal.

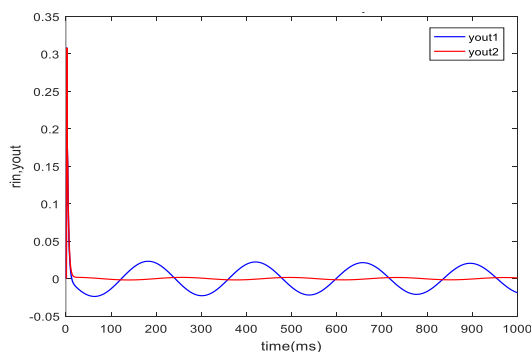


Fig. 18. Improved track sin sine signal.

From the comparison of Figs 17 and 18, it can be seen that when the looper system is affected by factors such as strip temperature fluctuations and roll gaps, the PID-based decoupling control system will have relatively large constant amplitude oscillations under continuous external disturbances. And the decoupling control performance of the system is reduced. The decoupling control effect of RBF neural network is better than that of PID. And on the basis of the improved weed optimization algorithm to optimize the weights, the system response is controlled in a small range, so that the system has a high stability.

6. CONCLUSIONS

Based on the hot rolling theory, the state space model of looper system is established. Considering the coupling relationship between the dynamic of looper angle and the dynamic of strip tension, the model is established. The reference looper angle and position are linearized approximately, and the strip tension output is obtained. In addition, based on the establishment of the state space model, the RBF neural network is applied to the looper system. Then the improved weed algorithm is used to optimize the perceptron of RBF neural network. The simulation results show that the improved weed algorithm is better than other algorithms in terms of optimization range or convergence accuracy, so that the accuracy of the neural network can reach a higher accuracy at the initial moment. The PID decoupling system and RBF neural network decoupling system are simulated and analyzed. At the same time, comparing the anti-interference performance of PID decoupling system and RBF neural network decoupling system. The simulation results show that the proposed RBF neural network decoupling system can obtain better dynamic performance. It can better improve the coupling relationship between the loop tension and the height system of the hot tandem rolling, which reflects better robustness. However, there are still shortcomings in the research and analysis process. For example, the looper system has multiple variables, strong coupling, and large interactions with other devices, and the system model cannot be accurately established. At the same time, it is impossible to consider the uncertain factors in reality, and further improvement is needed in the following study.

REFERENCES

- Chen M X, Zhou D D, Zhang H (2021). Temperature and pressure control system of extruder based on RBF neural network. *Machine Tool and Hydraulics*, 49(5): 71-76.
- Dong W H, Sun X X, Lin Y (2007). Redesign and simulation of model reference robust control. *Journal of System Simulation*, 19(4): 799-804.
- Dun X H, Zhou J Z, Zeng X F (2018). Application of neural network model based on improved weed algorithm optimization in runoff forecasting. *Hydropower Energy Science*, 36(5): 17-20.
- Giri R, Chowdhury A, Ghosh A, et al (2010). A modified Invasive weed optimization algorithm for training of feed-forward neural networks. *IEEE International Conference on Systems Man and Cybernetics*, IEEE, 3166-3173.

- Li B Q, Fan X, Zhang D Q, Jiang G J (2016). Modeling and Fuzzy Sliding Decoupling Control of Looper Multivariable System. *2016 Chinese Control and Decision Conference (CCDC)*, 2485-2490.
- Li B Q, Wang J J, Wang L, Zhang S L (2020). Research and Analysis of Robust Decoupling Control of Hydraulic Looper System. *2020 Chinese Control and Decision Conference (CCDC)*, 390-395.
- Li B Q, Zhang S L, Wang J J, Wang L (2020). Application of RBF-PID to MN-AGC in Hot Continuous Rolling. *2020 Chinese Control and Decision Conference (CCDC)*, 1086-1091.
- Long Z Q, Hao A M, Cao C K (2004). Robust controller for maglev train with reduced parameter sensitivity Design. *Control Theory and Application*, 21(3): 804-808.
- Mehrabian A R, Lucas C.A (2006). novel numerical optimization algorithm inspired from weed colonization. *Ecological Informatics*, 1(4):355-366.
- Peng B, Hu C G, Zhao R Z (2013). Neural network optimization strategy based on hybrid weed algorithm. *Vibration, Testing and Diagnosis*, 33(4):634-639
- Price K, Storn R M, Lampinen J A (2006). Differential evolution: a practical approach to global optimization. *Springer Science & Business Media*.